Article

Not peer-reviewed version

Functionalization of 3D Printed Polylactic Acid by Supercritical CO_2 Impregnation with Mango Leaf Extract and Evaluation with Endothelial Colony Forming Cells and Mesenchymal Stromal Cells

Ismael Sánchez-Gomar *, Mercedes Cáceres Medina, Cristina Cejudo-Bastante, Casimiro Mantell-Serrano, Lourdes Casas-Cardoso, Mª Carmen Durán-Ruíz *

Posted Date: 2 March 2026

doi: 10.20944/preprints202603.0072.v1

Keywords: PLA; supercritical carbon dioxide; supercritical impregnation; 3D-printing; mango leaf extract; polyphenols; DPPH; AAI; ECFCs; MSCs

 doi:10.20944/preprints202603.0072.v1

Article

Functionalization of 3D Printed Polylactic Acid by Supercritical CO_2 Impregnation with Mango Leaf Extract and Evaluation with Endothelial Colony Forming Cells and Mesenchymal Stromal Cells

Ismael Sánchez-Gomar [1,2,*], Mercedes Cáceres Medina [1], Cristina Cejudo-Bastante [3], Casimiro Mantell-Serrano [3], Lourdes Casas-Cardoso [3,†] and Mª Carmen Durán Ruiz [1,2,*,†]

[1] Department of Biomedicine, Biotechnology and Public Health, Faculty of Medicine, University of Cádiz. Plaza Falla 9, 11003 Cádiz, Spain

[2] Biomedical Research and Innovation Institute of Cadiz (INiBICA), 11002 Cádiz, Spain

[3] Chemical Engineering and Food Technology Department, Faculty of Science, Wine and Agrifood Research Institute (IVAGRO), University of Cadiz, Avda. República Saharaui, s/n, 11510 Puerto Real, Spain

* Correspondence: ismael.sanchez@gm.uca.es (I.S.G.), maricarmen.duran@gm.uca.es (M.C.D.R.)

† These authors contributed equally to this work.

Abstract

Poly(lactic acid) (PLA) devices can be functionalized with plant derived bioactives to introduce antioxidant activity while maintaining manufacturability and cytocompatibility. Here, a polyphenol rich mango leaf extract (MLE) was obtained by enhanced solvent extraction and incorporated into PLA using supercritical carbon dioxide assisted impregnation. Two manufacturing sequences were compared: impregnation after three dimensional (3D) printing of discs and impregnation of filaments prior to printing. Extract yield and radical scavenging capacity were quantified, and impregnation efficiency was assessed as a function of pressure and temperature. Biological performance was evaluated using adipose tissue derived endothelial colony forming cells (ECFCs) and adipose tissue derived mesenchymal stromal cells (MSCs), cultured separately and in co culture on functionalized substrates. Impregnation after printing provided higher and more reproducible loading while preserving disc geometry, whereas impregnation before printing promoted swelling and printing associated deformation that compromised structural fidelity. Cell based analyses supported improved adhesion, spatial distribution and proliferative status on discs produced by impregnation after printing under low temperature and high pressure conditions, without evidence of selective loss of either population in co culture by flow cytometry. These results support post print supercritical impregnation as a robust route to generate antioxidant, cell supportive PLA scaffolds from agricultural by products with potential relevance for vascular oriented biomedical applications.

Keywords: PLA; supercritical carbon dioxide; supercritical impregnation; 3D-printing; mango leaf extract; polyphenols; DPPH; AAI; ECFCs; MSCs

1. Introduction

Biodegradable polymers have emerged as revolutionary materials in the biomedical sector, offering innovative solutions for a wide range of applications. Unlike traditional polymers, these materials are designed to degrade in a controlled manner in the biological environment, transforming into biocompatible, non-toxic products that can be metabolized or excreted by the body[1]. This key feature eliminates the need for a second surgical procedure to remove the implant or device, reducing patient trauma and healthcare costs [2].

 doi:10.20944/preprints202603.0072.v1

The most prominent biodegradable polymers in biomedicine include poly(lactic acid) (PLA), used in sutures [3], bone implants [4], stents [5] and drug delivery [6]; poly(glycolic acid) (PGA), mainly for sutures [7]; and its copolymer poly(lactide-co-glycolide) (PLGA), widely used in drug delivery systems [8]) and tissue engineering [9]. Polycaprolactone (PCL) is used for long-term applications such as implants and tissue scaffolds [10–13]. Polydioxanone (PDO) is widely used in sutures and surgical staples [14,15]. Polyhydroxyalkanoates (PHAs) are being investigated for cardiovascular applications and nerve repair [16,17]. Finally, modified natural polymers such as chitosan and collagen are used in wound dressings and tissue engineering [18]. The aim is to provide biocompatible solutions that are safely degraded in the body.

The addition of substances with pharmacoactive properties to polymeric biomedical devices offers advantages in terms of the assimilation of these endoprostheses when implanted in a patient's body. Polymeric drug impregnation is a key strategy in the development of more effective therapies with fewer side effects, allowing controlled and sustained drug release at the desired site of action. The addition of natural substances with pharmacoactive properties to polymeric biomedical devices would provide beneficial regarding the assimilation of these endoprostheses when implanted into a patient's body. Several manufacturing processes have been developed to produce drug-eluting polymer implants and to control the release of the active compound, such as hot melt extrusion [19], solvent-casting, the creation of a coating containing the active compound on the surface of an already manufactured implant [20] or by soaking it into an active compound solution [21]. However, these traditional processes generally suffer either from high processing temperatures that can deteriorate thermosensitive active compound or from the use of organic solvents that must then be removed through numerous purification steps to respect FDA's requirements. Therefore, new methodologies to overcome these recognized drawbacks have been developed. In this context, the use of supercritical fluids provides several advantages over conventional methods because of their intermediate properties between those of a gas and a liquid, and considering that they present zero surface tension. Among the supercritical fluids, supercritical CO_2 ($scCO_2$) (critical temperature 31.1 °C and critical pressure 73.8 bar) is a non-toxic and non-flammable compound that produces formulations and materials without toxic traces [22,23].

The $scCO_2$-assisted impregnation has been used to incorporate drugs such as cefazolin into bone chips to prevent infection in orthopaedic procedures [24]; ibuprofen into gelatin-siloxane cryogels suitable for controlled drug release and tissue engineering [25]; ketoprofen into mesoporous silica [26] and moxifloxacin in contact lenses to treat keratitis [27], among others. Another application of $scCO_2$ impregnation is the incorporation of bioactive natural extracts into polymers used in biomedicine. Previous results evaluated the impregnation of olive leaf extract into biomedical filaments of thermoplastic polyurethane (TPU) and PLA in the range of 100-400 bar and temperatures of 35–55 ºC. TPU showed an extract load and antioxidant activity approximately 4 times higher than PLA under optimal operating conditions [28]. The use of winemaking by-products to functionalize PLA for biomedical applications has also been successfully studied. For impregnated filaments, the impregnation load was particularly dependent on the extract, providing up to 8% (extract mass/polymer mass) impregnation [29]. In addition, extracts obtained from (Mangifera indica L.) mango leaves (MEL) are a source of bioactive compounds with recognized biological activity. One of the most abundant compounds isolated from their leaves is mangiferin, a metabolite that has been shown to present anti-inflammatory and antioxidant properties in several studies [30]. Besides, mangiferin has also shown to reduce the apoptosis of cardiomyocytes during heart failure [31]. A previous study examines the potential of natural antioxidants extracted from mango leaves on the therapeutic capacity of endothelial colony forming cells (ECFC), which are considered promising for revascularization of ischemic areas in atherosclerotic patients in the treatment of cardiovascular diseases. The findings indicate that low concentrations of MLE improved angiogenic capacities of ECFCs and reduced proliferation, apoptosis, and the inflammatory response of these cells. Therefore, treatment of ECFCs with MLE could be a useful strategy to improve cell therapy in pathological settings [32]. The $scCO_2$-assisted impregnation of PLA with MEL was also investigated. The results

 doi:10.20944/preprints202603.0072.v1

confirm that PLA is an excellent material for delivering anti-denaturing and antioxidant compounds to the patient's body, although further in vitro and in vivo research are required [33]. In this regard, Grosso et al, 2023 evaluated supercritical fluid impregnation in two different configurations: (a) PLA filaments impregnated with MEL and then used in 3D printing (SCI + 3D); (2) 3D printed discs with PLA filaments that were then impregnated with $scCO_2$ (3D + SCI). The best results in terms of cell viability of ECFCs were obtained with the 3D + SCI configuration impregnated at low temperature (35 °C). The cells exhibited an elongated polygonal morphology, characteristic of healthy proliferating endothelial cells. This morphology suggests that the extract provides an optimal environment for growth and maintenance of the culture.

In this study, we aimed to evaluate the feasibility and biological performance of mango leaf extract functionalized PLAs produced by combining $scCO_2$ impregnation with 3D-printing. First, mango leaf extract was obtained by enhanced solvent extraction and characterized in terms of yield and antioxidant capacity using the 2,2-diphenyl-1-picrylhydrazyl (DPPH) assay and the antioxidant activity index. Second, the extract was incorporated into PLA by comparing two manufacturing sequences: impregnation after printing of discs and impregnation of filaments prior to printing, under defined pressure and temperature conditions, and loading was quantified gravimetrically. Third, we assessed the ability of the functionalized materials to support ECFCs and mesenchymal stromal cells (MSCs) in monoculture and in co culture using quantitative fluorescence microscopy, flow cytometry-based discrimination of cell populations, and proliferation and apoptosis readouts. This integrated design provides a direct comparison of manufacturing sequences and operating conditions, enabling the identification of process parameters that maximize loading while preserving print fidelity and cellular compatibility, thereby contributing to the valorization of mango leaf by products through a green processing strategy.

2. Materials and Methods

2.1. Raw Material and Chemicals

Mangifera indica L., Kent variety, leaves were provided by the "Estación Experimental La Mayora", Centro Superior de Investigaciones Científicas (CSIC), Málaga, Spain. The leaves were dried at room temperature to constant weight and stored in the absence of light. For the impregnation process, 1.75 mm diameter polylactic acid (PLA) filaments were purchased from Mundo Reader S.L. (Madrid, Spain).

For extraction and impregnation operations, carbon dioxide (99.99%) was supplied by Carburos Metálicos, S.A. (Sant Esteve Sesrovires, Spain), and ethanol (96.49%) was provided by Alcoholes del Sur, S.A. (Córdoba, Spain). 2,2-Diphenyl-1-picrylhydrazyl (DPPH), purchased from Sigma-Aldrich (Steinheim, Germany), was used to evaluate antioxidant capacity. HPLC-grade formic acid (98%) and acetonitrile were supplied by Panreac Química S.L.U. (PanReac AppliChem ITW Reagents; Barcelona, Spain).

2.2. Enhance Solvent Extraction (ESE)

Extractions were performed using a Thar Technologies SF1000 system (Pittsburgh, PA, USA), equipped with a 1 L extractor and two high-pressure pumps (max. flow rate of 50 g/min each) for the independent delivery of CO_2 and ethanol. Process parameters were precisely managed via an automatic back-pressure regulator and a thermostatic jacket to maintain thermal stability. The system layout is illustrated in Figure 1.

For the sample preparation, mango leaves were crushed to a particle size of 2–3 mm. A 200 g of the plant material was loaded into a paper cartridge and placed within the high-pressure vessel, which contained 500 mL of ethanol. Ethanol was selected as the co-solvent due to its eco-friendly nature, low toxicity, and proven efficiency in recovering polyphenolic compounds. The extraction was initiated by pressurizing the system with CO_2 at a constant flow of 10 g/min until reaching 200 bar. Following the methodology described in previous studies [34], the process was conducted in

 doi:10.20944/preprints202603.0072.v1

batch mode at 80 °C for 24 h. Upon completion, the system was depressurized, and the resulting extract was collected and stored at 4 °C in the dark to ensure stability. All procedures were performed in duplicate to ensure reproducibility.

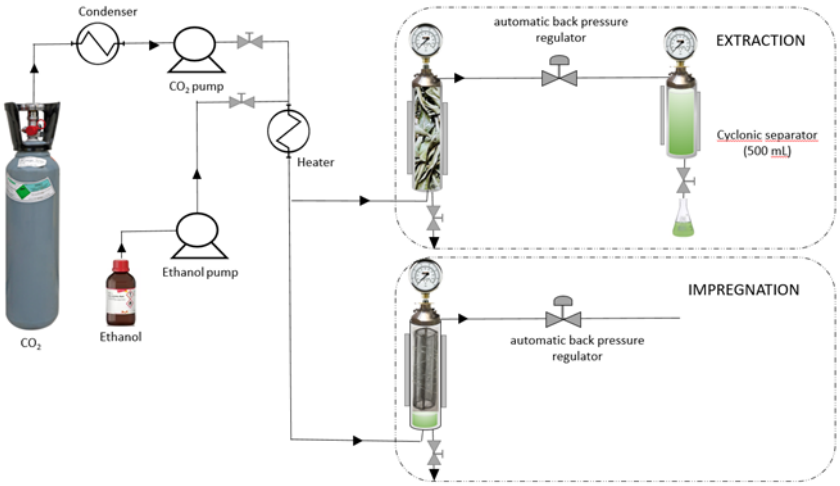

Figure 1. Schematic diagram of the extraction and impregnation processes.

2.3. Characterization of the Extracts

The extract was characterized in terms of total extraction yield, antioxidant activity, and the quantity of phenolic compounds. The extraction yield (%Y) was calculated as the ratio of the total dry extract mass (md) divided by the initial mass of the leaves (mi) according to Eq. 1:

$$\%Y = \frac{m_d}{m_i} * 100 \quad (1)$$

The extraction yields were determined in duplicate.

The antioxidant capacity of the extract was determined following free radical scavenging method of DPPH (2,2-diphenyl-1-picrylhydrazyl) [35]. These species, characterized by the presence of unpaired electrons in its external orbital, are susceptible to interacting with compounds that present antioxidant activity through the cession of a hydrogen atom. The reduction of this compound leads to a change from purple to yellow color, with the subsequent drop of absorbance, which was detected spectrophotometrically at 515 nm maximum absorbance.

For the DPPH assay, 293 µL of 60 µM DPPH ethanolic solution was added to 7 µL extract aliquots at different concentrations (48–2400 µg/mL) in ethanol. After 2 h of incubation at room temperature in the absence of light, the absorbance was measured at 515 nm using a spectrophotometer (Cary 60 UV-Vis de Agilent Technologies). A control experiment was also conducted by replacing the 7 µL extract with ethanol. The percentage of inhibition of the oxidation (%I) was calculated by comparing the absorbance of the control (A_0) against the absorbance measured after 2 h (Ai) according to Eq 2:

$$\%\, I = \frac{(A_0 - A_i)}{A_0} * 100 \quad (2)$$

The half maximal inhibitory concentration (IC_{50}), defined as the extract concentration required to inhibit oxidation by 50%, was graphically determined by plotting the percentage inhibition (%I) against the extract concentration. Lower IC_{50} values indicate higher antioxidant capacity.

The result also was expressed in terms of antioxidant activity index (AAI). This index was defined by Scherer and Godoy, 2009 [36] as the quotient between the initial DPPH concentration in the reaction and the efficient concentration (IC_{50}) (Eq. 3). The assay was carried out in duplicate, and the standard deviation was estimated.

$$\text{AAI} = \frac{[\text{DPPH}]\ (\frac{\mu g}{mL})}{IC_{50}\ (\frac{\mu g}{mL})} \quad (3)$$

 doi:10.20944/preprints202603.0072.v1

The main phenolic compounds in MEL were quantified by HPLC as previously described [34], using a Jasco Corporation system (Madrid, Spain). Separation was achieved on a Fortis C18 column (150 mm × 3 mm, 5 μm; Fortis Technologies Ltd.), also supplied by Jasco Corporation. The mobile phase consisted of 0.1% formic acid in water (solvent A) and 0.1% formic acid in acetonitrile (solvent B). The injection volume for all samples was 20 μL. The mobile phase was eluted at a flow rate of 1 mL/min using a linear gradient as follows [t (min), %B]: (0, 0), (0.2, 0), (0.3, 7), (14.7, 8.5), (40, 19), (45, 33), (48, 50), (50, 95), (57, 0), and (63, 0). Data acquisition and processing were performed using Jasco ChromNAV software (version 2.04.04). The assay was performed in duplicate and results were expressed as mean ± standard deviation.

2.4. 3D Printing

Discs were printed using Ultimaker Cura computer software and an ANYCUBIC Mega S 3D printer. The printing temperature was 200 °C and the printing rate was 25 mm/s. Two different configurations were evaluated using the methodology proposed by Grosso et al., 2022. The first configuration involves printing PLA discs and then impregnating them with $scCO_2$ in the presence of MLE as the active extract (3D+SCI). The second configuration involves impregnating a PLA filament with MLE, followed by printing discs with this filament. This configuration is called SCI+3D.

2.5. Impregnation at High Pressure (SCI)

Impregnation of MLE into PLA using $scCO_2$ was carried out using high-pressure equipment from Thar Technologies (Pittsburgh, PA, USA), similar to that used in the extraction process (Figure 1). The SF100 model, featuring a 100 mL vessel, was used to impregnate the 3D+SCI discs. In contrast, the SF1000 model (1 L capacity) was used for the SCI+3D discs, which were impregnated in their original filament conformation prior to printing. The primary difference between the setups was the volume of the vessel and the amount of initial PLA added; other components, such as pumps and heat exchangers, were similar.

For the impregnation, the extract was added to the bottom of the vessel at a volume corresponding to 3% of the reactor's capacity. To prevent direct contact between the polymer and the extract, the PLA filaments or discs were placed in a steel support basket. The process was conducted in batch mode: CO_2 was first pumped at a flow rate of 10 g/min until reaching the target pressure. The flow was then stopped, and the pressure was maintained throughout the impregnation period. Finally, the system was rapidly depressurized (40 bar/min) to facilitate impregnation of the PLA.

Any excess extract was removed from the filaments using a damp lint-free cloth (o moist tissue). Experiments were performed in duplicate, and the impregnated samples were stored in the dark to prevent degradation.

To evaluate the influence of processing conditions, two pressure levels (100 and 400 bar) and two temperatures (35 and 55 °C) were tested, covering a wide range of CO_2 densities. At 35 °C, the CO_2 density values were 700.1 and 972.2 kg/m³ at pressures of 100, and 400 bar, respectively. At 55 °C, the corresponding values were 337.2 and 906.8 kg/m³. The experiments were conducted for 1 h.

2.6. Characterization of the Impregnated Polymers

To determine the MLE loading on the impregnated polymer, the samples were chemically dissolved in dichloromethane (CH_2Cl_2). The absorbance of the resulting solutions was then quantified using a UV-VIS spectrophotometer (UV Mini-1240, Shimadzu, Japan).

A calibration curve was initially established using extract concentrations ranging from 32 to 900 mg/mL in 3 mL of CH_2Cl_2. To account for potential matrix effects, a fixed amount of neat polymer (60 mg) was added to each standard solution, ensuring that the polymer's presence did not interfere with the readings. The measurements were performed at 660 nm, as this wavelength corresponds to the extract's maximum absorbance while minimizing interference from other components in the medium.

 doi:10.20944/preprints202603.0072.v1

The final concentration was calculated from the corresponding calibration curve in the same solvent (Eq. 4)

$$y = 0.0017 * C - 0.057 \qquad R^2 = 0.9961 \qquad (4)$$

where C is the MEL concentration, mg/ml. Finally, the loading percentage (% L) was calculated from Eq. 5:

$$\%L = \frac{m_{MLE}}{m_{POL}} * 100 \qquad (5)$$

where mMLE is the mass of extract impregnated (g) and mPOL is the mass of the polymer (g) employed in each assay. All experiments were performed in duplicate.

The morphological changes of impregnated PLA were observed by scanning electron microscopy (SEM) using a Nova NanoSEM 450 microscope (FEI, Hillsboro, OR, USA). The samples were cut into small pieces using a cutting plier and then, were coated with a thin layer of gold (10 nm) using a Cressington Sputter Coater model 208 HR from Cressington Scientific Instrument (Watford, UK) for better conductivity and imaging.

2.7. Isolation and Culture of ECFCs and MSCs

Both ECFCs and MSCs were obtained from white adipose tissue, as previously described by Lin et al. (2013)[37]. Briefly, ECFCs were seeded on plates coated with 1% gelatin (Sigma-Aldrich, St. Louis, MO, USA) and cultured in EGM-2 basal medium (Lonza, Basel, Switzerland), excluding hydrocortisone, supplemented with 20% fetal bovine serum (Gibco, Thermo Fisher Scientific, Waltham, MA, USA) and 1× glutamine-penicillin-streptomycin (Gibco, Thermo Fisher Scientific, Waltham, MA, USA). MSCs were cultured in MSC Growth Medium 2 (PromoCell, Heidelberg, Germany) supplemented with 10% FBS (Gibco, Thermo Fisher Scientific, Waltham, MA, USA) and 1× GPS (Gibco, Thermo Fisher Scientific, Waltham, MA, USA). Cell characterization was performed as previously described by Sánchez-Gomar et al.[32]. All cell populations were used between passages 5 and 7.

2.8. Cell Viability

To evaluate the viability of ECFCs and MSCs cultured on PLA discs impregnated with mango leaf extract (MLE), 50,000 cells of each cell type were seeded onto the discs and maintained for 72 h in EBM-2 complete medium (Lonza, Basel, Switzerland). Cell adhesion and spatial distribution were assessed by Calcein staining (Calcein, Sigma-Aldrich, St. Louis, MO, USA) and quantified by fluorescence microscopy. Calcein-positive cells were counted and normalized to surface area (cells per mm²) using image-based analysis. Based on previous results from our group [38], cell assays were performed using the disc conditions described above, in triplicate. Quantification of adherent cells was performed using Fiji ImageJ software (National Institutes of Health, Bethesda, MD, USA), enabling the identification of the impregnation condition that most effectively supported the growth of each cell type.

2.9. Flow Cytometry Based Quantification of ECFCs and MSCs

To distinguish ECFCs from MSCs adherent to PLA discs, flow cytometry analysis was performed using CD31 as an endothelial-associated surface marker (anti-human CD31 antibody, BioLegend, San Diego, CA, USA; Cat. 303103). Briefly, 50,000 ECFCs and 50,000 MSCs were co-seeded onto PLA discs corresponding to conditions 1 and 2 and incubated for 72 h in EGM-2 complete medium (Lonza, Basel, Switzerland) supplemented with 20% FBS (Gibco, Thermo Fisher Scientific, Waltham, MA, USA) and 1% glutamine-penicillin-streptomycin (Gibco, Thermo Fisher Scientific, Waltham, MA, USA). After incubation, cells were detached from the discs using trypsin (Gibco, Thermo Fisher Scientific, Waltham, MA, USA) and stained with anti-CD31 antibody for 30 min. Samples were acquired on a CytoFLEX flow cytometer (Beckman Coulter, Brea, CA, USA), collecting the entire cell suspension to quantify the proportion of CD31-positive cells relative to total events.

 doi:10.20944/preprints202603.0072.v1

Experiments were performed in triplicate. Data were analyzed using CytExpert software (Beckman Coulter, Brea, CA, USA) and FlowJo software (BD Biosciences, Ashland, OR, USA).

2.10. Proliferation Assay

ECFCs and MSCs were seeded at 50,000 cells per well in 24-well plates containing PLA discs from the selected optimal condition 2 (impregnation after printing, 35 °C, 400 bar), and subsequently discs from condition 1 (impregnation after printing, 35 °C, 100 bar). Cultures were maintained in 500 µL of basal EGM-2 medium for 72 h at 37 °C in a humidified atmosphere with 5% CO_2. All experiments were performed in triplicate.

After 72 h, cells were washed with 1× PBS (Gibco, Thermo Fisher Scientific, Waltham, MA, USA), fixed with 4% paraformaldehyde, and permeabilized with 0.2% Triton X-100 (Sigma-Aldrich, St. Louis, MO, USA) in 1× PBS (0.2% PBT) for 30 min under gentle agitation. Samples were blocked with 2.5% bovine serum albumin (BSA) (Sigma-Aldrich, St. Louis, MO, USA) in 0.2% PBT and incubated overnight at 4 °C with rabbit anti-Ki67 primary antibody (PA5-16785; Invitrogen, Thermo Fisher Scientific, Waltham, MA, USA) diluted 1:500 in 2.5% BSA. Samples were then incubated for 1 h at room temperature in the dark with Alexa Fluor 488-conjugated anti-rabbit secondary antibody (A-11008; Thermo Fisher Scientific, Waltham, MA, USA) diluted 1:1000, followed by nuclear counterstaining with 4′,6-diamidino-2-phenylindole (DAPI) (Sigma-Aldrich, St. Louis, MO, USA) diluted 1:5000 in 2.5% BSA.

Images were acquired at 10× magnification using an Olympus IX81 fluorescence microscope (Olympus Corporation, Tokyo, Japan). Quantification was performed using ImageJ software. DAPI staining was used to determine the total number of nuclei, and Ki67 positivity identified proliferating cells. Proliferation was expressed as the percentage of Ki67-positive nuclei relative to total DAPI-positive nuclei for each experimental condition.

2.11. Apoptosis Assay

To assess whether incorporation of mango leaf extract into PLA discs modulated apoptosis in ECFCs and MSCs, flow cytometry was performed using Annexin V (Cat. 560506; BD Biosciences, San Jose, CA, USA) and propidium iodide (Cat. 556463; BD Biosciences, San Jose, CA, USA). Annexin V and propidium iodide staining enabled discrimination of viable cells (Annexin V-negative, propidium iodide-negative), early apoptotic cells (Annexin V-positive, propidium iodide-negative), and late apoptotic or necrotic cells (Annexin V-positive, propidium iodide-positive).

Cells were seeded under the same conditions described above and analyzed after 72 h of culture. Following incubation, cells were harvested and stained with Annexin V and propidium iodide according to the manufacturer's instructions. Samples were acquired on a CytoFLEX analytical flow cytometer (Beckman Coulter, Brea, CA, USA), and experiments were performed in triplicate. Data were processed using FlowJo software (BD Life Sciences, Ashland, OR, USA).

2.12.. Statistical Analysis

Statgraphics Centurion 18 software was used to analyze extract loading in impregnated PLA. Analysis of variance was performed, and results were represented using a Pareto chart to identify the most influential variables affecting the impregnation process.

For cell-based assays, GraphPad Prism 9 was used. Normality was assessed using the Shapiro Wilk test, and homogeneity of variances was evaluated using the Brown Forsythe test. For datasets meeting parametric assumptions, group comparisons were performed using analysis of variance followed by Tukey post hoc testing for pairwise comparisons. For datasets not meeting parametric assumptions, the Kruskal Wallis test was used for multiple group comparisons and the Mann Whitney U test was used for pairwise comparisons where appropriate. A two tailed significance level of 0.05 was applied.

 doi:10.20944/preprints202603.0072.v1

3. Results and Discussion

3.1. Characterization of Mango Leaf Extract

Enhanced solvent extraction (ESE) was explored in this work as a technique to obtain MLE with high antioxidant content. Although bioactive compounds have traditionally been recovered from plants using conventional extraction methods, the increasing demand for safety in the food, cosmetic, biomedical, and pharmaceutical industries, driven by consumer health and environmental protection, has prompted the search for more efficient and sustainable processes. In this context, this work examined an eco-friendly extraction technique based on high-pressure technologies. Increasing the pressure enhances the contact surface area between the matrix and the solvent, allowing the solvent to penetrate areas of the solid matrix that would not normally be accessible at ambient pressure. Furthermore, increasing the extraction temperature promotes the release of analytes from the solid matrix and their diffusion into the solvent, resulting in higher partition coefficient values [39]. Another advantage of ESE is the use of high proportions of CO_2, which reduces the consumption of liquid solvents. However, the presence of ethanol is essential to recover high-to-medium polarity bioactive compounds, such as mangiferin, quercetin, and gallic acid [40].

A maximum global extraction yield of 10.83 ± 0.91% (w/w, dried leaves) was obtained using CO_2/ethanol (1:1 v/v) at 200 bar and 80 °C (Table 1). According to the literature [36], plant extracts show poor antioxidant activity when AAI < 0.5, moderate activity between 0.5 and 1.0, strong activity between 1.0 and 2.0, and very strong activity when AAI > 2.0. The obtained extract presented an AAI value of 2.36 ± 0.01, corresponding to a very strong antioxidant capacity. This high activity is in agreement with the high total polyphenol content, which includes major phenolic compounds such as mangiferin, iriflophenones, and gallic acid (Table 1).

Table 1. Characterization of the extract

Yield extraction (%)	10.83 ± 0.91
IC_{50} (μg/mL)	9.74 ± 0.03
AAI	2.36 ± 0.01
Phenolic compounds (g/100 g dried extract)	
gallic acid	2.57 ± 0.04
mangiferin	9.08 ± 0.02
iriflophenone 3-C-β-d-glucoside	11.12 ± 1.03
iriflophenone 3-C-(2-O-galloyl)-β-d-glucoside	2.72 ± 0.05
quercetin 3-d-galactoside	1.87 ± 0.08
quercetin 3-β-d-glucoside	1.52 ± 0.02

Results are expressed as the mean value ± standard deviation of the assays carried out in duplicate.

A previous work [38] evaluated the same extraction technique under the same operating conditions, obtaining a similar extraction yield of 10.7%, with lower AAI (AAI = 0.7703) than reported here. The AAI presented in this study is considerably higher than that reported in the previous publication. This confirms that the MLE obtained has a potent antioxidant capacity that could be beneficial in biomedicine. It is known that the extraction method and the climatic conditions in which the plant grows both have an important influence on the extraction yield [41], and it seems that it is the latter factor that has caused the increase in antioxidant activity in the extract obtained.

3.2. Supercritical Impregnation

The Supercritical Solvent Impregnation (SSI) process typically follows three distinct stages: (1) dissolution of the target compounds in $scCO_2$; (2) saturation of the solid matrix with the solutes; and

 doi:10.20944/preprints202603.0072.v1

(3) system depressurization for $scCO_2$ removal. In the first stage, $scCO_2$ serves as the solvent for the target compounds. Simultaneously, it diffuses into the carrier material, inducing swelling and plasticization, which enhances mass transfer. The solubility of the solutes in the supercritical phase is governed by their chemical nature, as well as the operational pressure and temperature. During the second stage, the equilibrium between $scCO_2$, the solutes, and the solid matrix is critical for successful adsorption. For effective impregnation, the affinity between the target compounds and the solid matrix must surpass their affinity for the supercritical solvent. This favorable interaction ensures the migration of the solutes from the supercritical phase onto the adsorbent's surface or into its pores. This phase also depends on the pressure and temperature conditions used. In the final stage, the system is depressurized, causing CO_2 revert to a gas, which is then removed from the system and potentially recycled. As a result, the target compounds can be impregnated on the solid matrix [42].

Figure 2 shows the results obtained by operating at different pressure and temperature values. Two distinct processing sequences were evaluated: (i) filament impregnation followed by 3D printing (SCI + 3D, Figure 2I and 2III), and (ii) post-printing impregnation of the discs (3D + SCI, Figure 2II). The core objective of comparing these methodologies and their respective operating conditions is to determine their subsequent impact on cell culture performance.

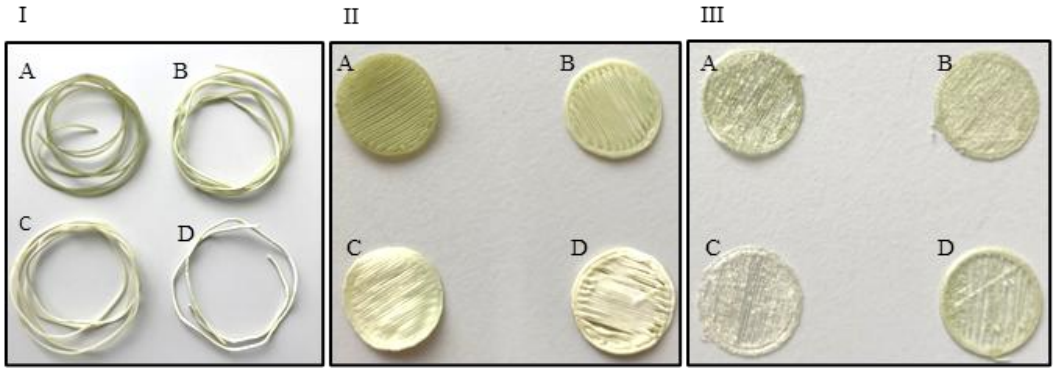

Figure 2. (I) Impregnated PLA filaments; (II) 3D-printed discs + SCI; and (III) SCI + 3D-printed discs impregnated under the following conditions: (A) T = 35 °C, P = 100 bar; (B) T = 35 °C, P = 400 bar; (C) T = 55 °C, P = 100 bar; and (D) T = 55 °C, P = 400 bar.

Comparing Figures 2II and 2III shows that the discs in the latter are more deformed under all impregnation conditions than those in Figure 2II. During impregnation, the polymer's free volume increases due to its plasticization, a process known as swelling. This can result in variations in the diameter and length of the filament. Since the filament is fed into the printer, the swelling effect may render it unsuitable for printing purposes. The results obtained agree with those previously observed [29,33,38] and are important in avoiding an excessive increase in the polymer's diameter, as this causes impediments in the printing process.

Figure 3A shows MEL loading (%) for the different operating conditions studied. The values range from 0.61 to 0.97% for the 3D + SCI configuration, which is lower (from 0.21 to 0.41%) than for the other SCI + 3D configuration. Therefore, it can be inferred that the 3D + SCI configuration was preferable. In general, operating at 35 °C results in better impregnation performance than operating at 55 °C. An increase in temperature at constant pressure decreases the density of the $scCO_2$, and therefore the affinity of the compounds for the supercritical phase decreases. This results in a low $scCO_2$/active compound solution, meaning less of the active compound can come into contact with the polymer, hence the impregnation is lower. This effect is more pronounced in the 3D + SCI configuration than in the SCI + 3D configuration. On the other hand, the higher $scCO_2$ density at higher pressures and constant temperature, causes a better affinity of the compounds to the supercritical phase, leading to lower impregnation values.

 doi:10.20944/preprints202603.0072.v1

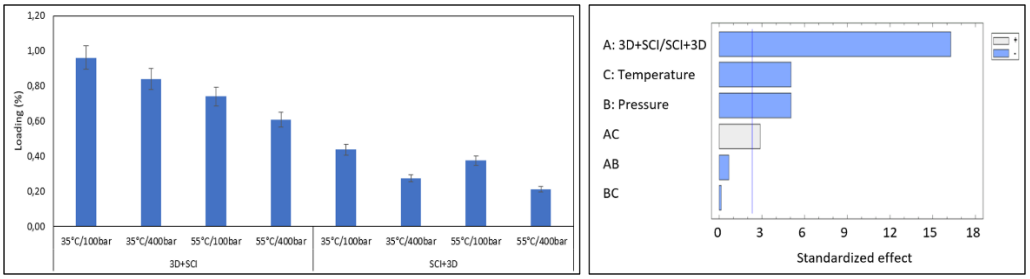

Figure 3. A) MLE loading at different impregnation conditions. Los valores se representan como media ± SEM (n=2). B) Pareto chart showing MLE loading.

The Pareto diagram (Figure 3B) obtained by statistically processing the design of the experiment confirms that there is a high correlation between the MLE loading and the operating conditions. The most influential factor was the manner in which the process is carried out (3D+SCI/SCI+3D). Pressure and temperature also have a negative effect, so working at 100 bar and 35 °C is advisable to obtain the highest loads. The interaction between temperature and pressure has been shown to significantly affect MLE loadings, probably due to the correlation between supercritical carbon dioxide ($scCO_2$) density and these two variables.

Filaments impregnated at 100–400 bar and 35 °C with 3D+SCI, SCI+3D, and non-impregnated filaments (PLA control) were observed under a microscope to detect any differences in the polymer surfaces before and after impregnation with MLE. Figure 4 shows the appearance of the filament surfaces.

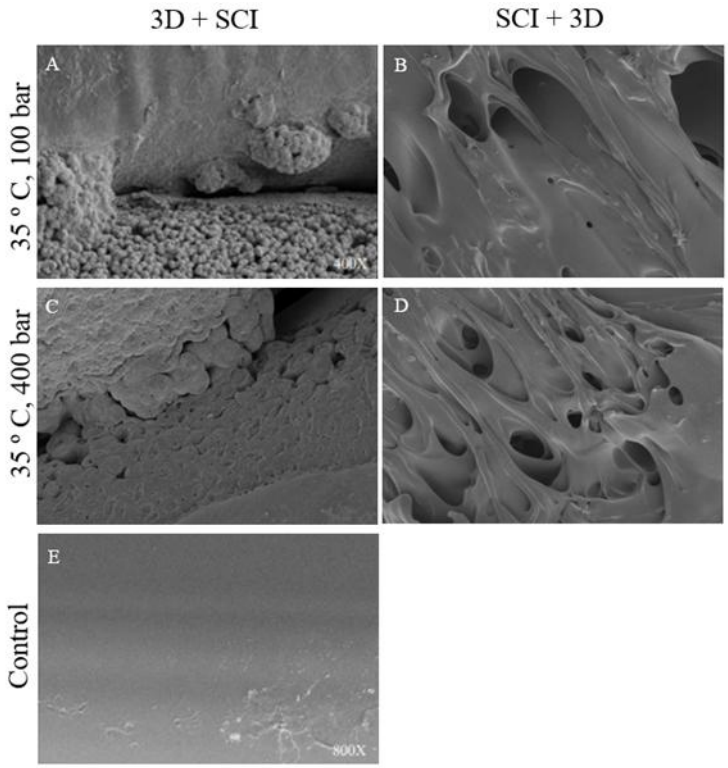

Figure 4. Scanning electron microscopy of the samples: (A) 3D + SCI, T= 35 º C, P= 100 bar (400X), (B) SCI + 3D, T= 35 º C, P= 100 bar (400X), (C) 3D + SCI, T= 35 º C, P= 400 bar (400X), (D) SCI + 3D, T= 35 º C, P= 400 bar (400X), (E,F) Unimpregnated PLA control disk (800X).

The unimpregnated PLA control discs (Figure 4E) have mostly a uniform and smooth surface. Hardly any irregularities were observed; those present may be intrinsic to the material. The 3D + SCI

 doi:10.20944/preprints202603.0072.v1

images (Figure 4A and C) differ significantly from the SCI+D images (Figure 4B and D). The 3D + SCI discs (Figure 4A and C) show the spherical-shaped mango leaf extract coating the inside and outside of the polymer. Bumps are also visible in both images, probably due to particles lodged inside the polymer, as well as some surface pores resulting from the polymer swelling in the presence of the extract [33].

In the case of the SCI + 3D discs (see Figures 4B and 4D), deformation of the polymer conformation was observed, and no MLE-impregnated particles are visible. This may be because the filament is impregnated before being introduced into the printer, which increases its porosity and causes the diameter to increase by a few millimeters. This deformation is evident when the filament passes through the 3D printer. These images show that the internal structure of the PLA filament has changed. Such alterations could result in critical mechanical malfunctions that could affect the subsequent performance of the polymer when used to manufacture medical devices.

3.3. Cell Viability

Cell viability and adhesion on MLE functionalized PLA discs were assessed after 72 h of culture by Calcein staining and fluorescence microscopy. The quantitative outcomes obtained for each condition are shown in Figures 5I, 7II and 7III. A clear and consistent pattern emerged across ECFCs, MSCs and ECFCs + MSCs co-culture. The most prominent difference was the markedly higher number of adherent cells on discs manufactured by printing first and impregnating afterwards (3D + SCI) at 35 °C, compared with the remaining conditions. Within this 3D + SCI group, an additional pressure dependent effect was observed, as discs impregnated at 400 bar supported a higher number of adherent cells than discs impregnated at 100 bar. This pressure associated increase was consistently detected in wells seeded with ECFCs, in wells seeded with MSCs, and in ECFCs + MSCs co culture. Importantly, all 3D + SCI conditions exhibited statistically significant differences relative to the unimpregnated PLA control discs in terms of adherent cell number (Figures 5I to 5III).

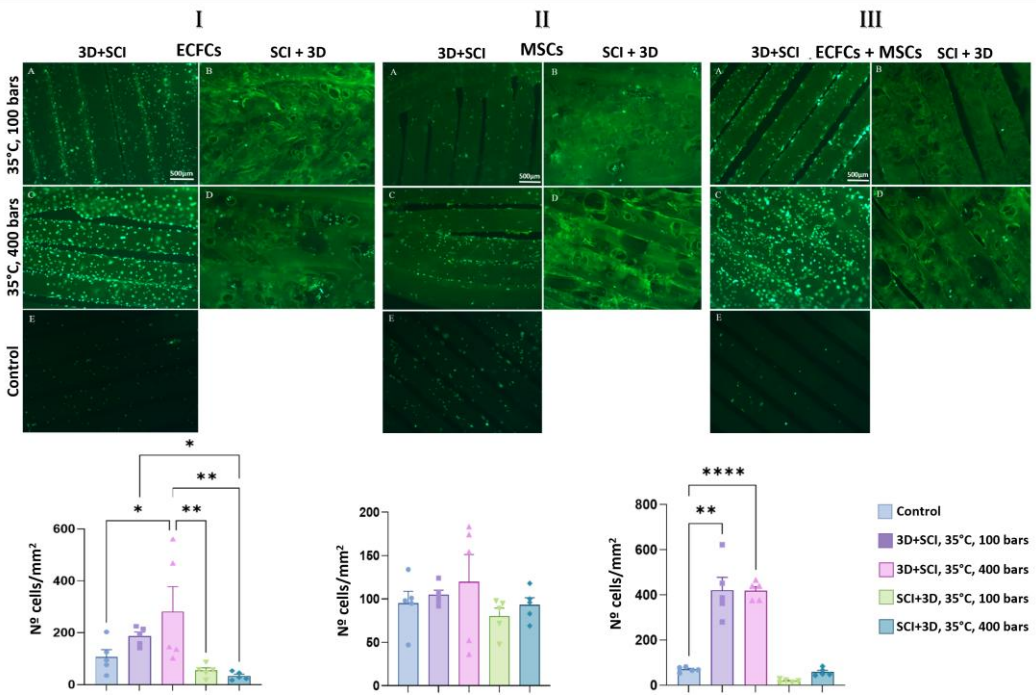

Figure 5. Viability of cultures on PLA discs impregnated with mango leaf extract under different conditions: (7.I) ECFCs, (7.II) MSCs, and (7.III) ECFCs + MSCs. (A) 3D + SCI, T = 35 °C, P = 100 bar; (B) SCI + 3D, T = 35 °C, P = 100 bar; (C) 3D + SCI, T = 35 °C, P = 400 bar; (D) SCI + 3D, T = 35 °C, P = 400 bar; (E) Control. Images were acquired using a fluorescence microscope with a 4X objective. Graphs show the number of cells counted per mm2 of PLA disc surface. Values are presented as mean ± SEM (n = 3). *p-value: ** < 0.01, **** < 0.0001.

 doi:10.20944/preprints202603.0072.v1

A notable change was observed when the polymer was impregnated prior to 3D printing (SCI + 3D). In this sequence, the impregnated filaments exhibited irregular and unstable surfaces that hindered disc fabrication. Consequently, the resulting SCI + 3D discs showed geometric deformation and loss of the original flat conformation, as illustrated in panels B and D of Figures 5I, 5II and 5III. Under these conditions, the presence of surface undulations led to non-uniform spatial distribution of adherent cells, which tended to concentrate in specific valley-like regions. This constrained colonization resulted in an overall reduction in the total number of cells adhering to the PLA discs [32].

In addition to the effects of material and processing, differences between cell types were apparent. MSC-seeded wells yielded lower adherent cell numbers than ECFC seeded wells across all conditions. This may reflect intrinsic differences in adhesion behavior, as endothelial cells possess multiple adhesion-related proteins and readily attach to common culture substrates such as collagen, fibronectin and tissue culture treated plastic, and can also attach, albeit less efficiently, to untreated glass [43]. Such inherent adhesion competence may become particularly relevant when surface geometry and topography are suboptimal, as in the SCI + 3D discs.

Calcein-based imaging not only enabled quantification of adherent cell density but also revealed condition dependent differences in cell morphology and spatial organization. Representative 10X fluorescence micrographs are shown in Figure 6. Under the 3D + SCI workflow at 35 °C and 400 bar, ECFCs exhibited an extended, well spread morphology consistent with the formation of a cohesive endothelial layer, whereas MSCs displayed a narrower, elongated spindle like shape, which is characteristic of healthy mesenchymal cells [44]. The observed morphology and spatial distribution suggest that MLE functionalization under these conditions provides a permissive microenvironment for cell attachment and maintenance, which may be linked to the bioactive properties of the extract, including the antioxidant activity reported above [45].

In contrast, for SCI + 3D discs (Figure 6C), where ECFCs + MSCs were seeded, the adherent cells did not exhibit the same spread morphology observed on 3D + SCI discs. Instead, their appearance was closer to that observed on unimpregnated control PLA discs (Figure 6D). Both conditions were characterized by a reduced number of adherent cells and a predominantly rounded, spherical morphology. Such contracted morphology is commonly associated with an unfavorable physiological state and has been linked to stress induced cellular senescence, where cells lose their typical shape and adopt a more rounded phenotype when the microenvironment is not supportive for adhesion and proliferation [46].

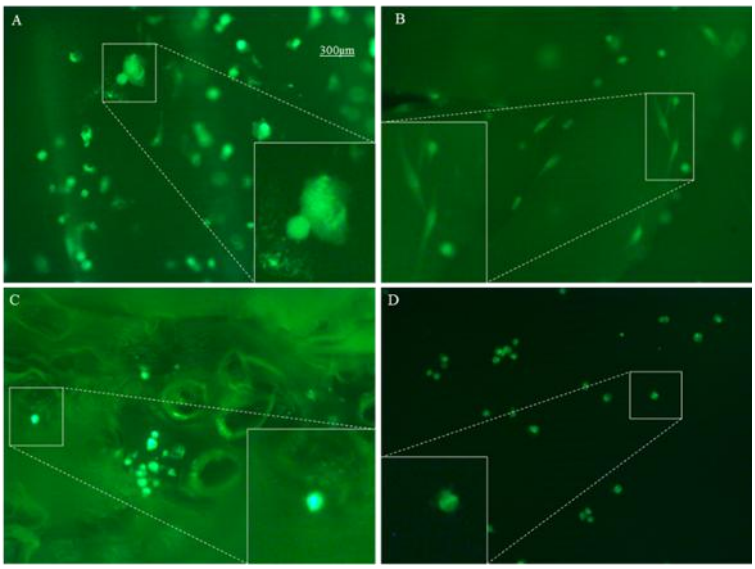

Figure 6. Analysis of cell morphology on PLA discs impregnated with mango leaf extract. Representative fluorescence microscopy images (10X objective) of ECFCs and MSCs cultured on PLA discs impregnated with MLE under different conditions, using an unimpregnated PLA disc as control: (A) ECFCs, T = 35 °C, P = 400 bar

 doi:10.20944/preprints202603.0072.v1

(3D + SCI); (B) MSCs, T = 35 °C, P = 400 bar (3D + SCI); (C) ECFCs + MSCs, T = 35 °C, P = 400 bar (SCI + 3D); (D) PLA control.

Overall, the contrast between 3D + SCI and SCI + 3D was evident at the morphological level. Although SCI + 3D discs were also processed in the presence of MLE, the resulting cell morphology resembled that of the non-impregnated controls, suggesting that impregnation prior to printing may compromise either the effective presentation of bioactive cues or the integrity of the polymer surface environment after printing. A plausible explanation is that the printing step, which involves high temperatures, may reduce antioxidant activity associated with polyphenolic compounds [47], while simultaneously altering the internal structure of the polymer and its loading profile. In agreement with the adhesion quantification, MLE impregnation increased both the number of adherent cells and the overall culture quality when impregnation was performed after printing (3D + SCI).

3.4. Proliferation, Cell Type Identification, and Apoptosis Assays

Based on the results of the previous viability assay, condition 2 (3D + SCI, 35 °C, 400 bar) followed by condition 1 (3D + SCI, 35 °C, 100 bar) were selected as the optimal processing strategies. Consequently, they were used for immunofluorescence analysis of the ECFCs + MSCs coculture. The results are shown in Figure 7.

The proliferation percentages were 56.74% for condition 1 (3D + SCI, 35 °C, 100 bar), 66.01% for condition 2 (3D + SCI, 35 °C, 400 bar), and 10.74% for the control discs. Both impregnated conditions showed statistically significant differences relative to the control. These findings indicate that condition 2 (35 °C, 400 bar) promoted the highest proliferative fraction. This is consistent with previous assays identifying this temperature-pressure setting as the most favorable condition for ECFCs and MSCs viability, which also correlated with higher impregnated extract levels

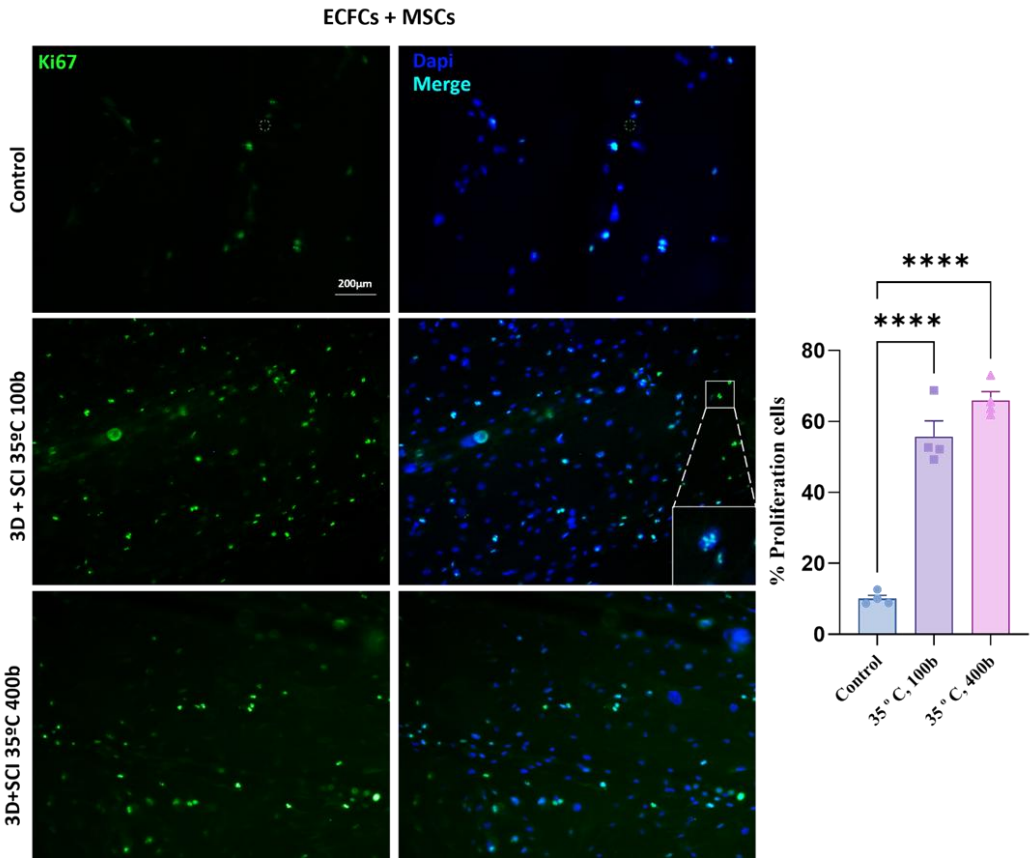

Figure 7. Effect of mango leaf extract on ECFCs + MSCs proliferation. Representative images of ECFCs + MSCs cultures on PLA discs impregnated with MLE under different conditions: (A) 3D + SCI, T = 35 °C, P = 100 bar; (B) 3D + SCI, T = 35 °C, P = 400 bar; (C) Control. Images were acquired using a fluorescence microscope with a

 doi:10.20944/preprints202603.0072.v1

10X objective and processed using Merge software. The graph shows the percentage of proliferating cells on PLA discs under the studied conditions. Values are presented as mean ± SEM (n = 3). P-value: **** < 0.0001.

In contrast to these results, several studies have reported anti proliferative properties of MLE. This apparent discrepancy may be attributed to the low MLE concentration achieved in the current system (0.0096 mg/L), compared with concentrations evaluated in previous reports [32]. Therefore, it would be of interest to further explore the concentration threshold at which MLE begins to exert anti-proliferative effects, as this could enable the modulation of cell growth on the polymer surface, ensuring optimal coverage of the biodegradable material while maintaining controlled proliferation [48].

In addition, a flow cytometry-based assay was carried out to corroborate the presence of the two cell types and to determine whether there were significant differences in their adherence to PLA discs. Thus, following flow cytometric quantification, the percentage of CD31+ cells was representative of the endothelial fraction relative to total cells (Figure 8A). The CD31− percentage, corresponding to the mesenchymal fraction, and the total cell number were also determined, as summarized in Figure 8B, 8C, and 8D.

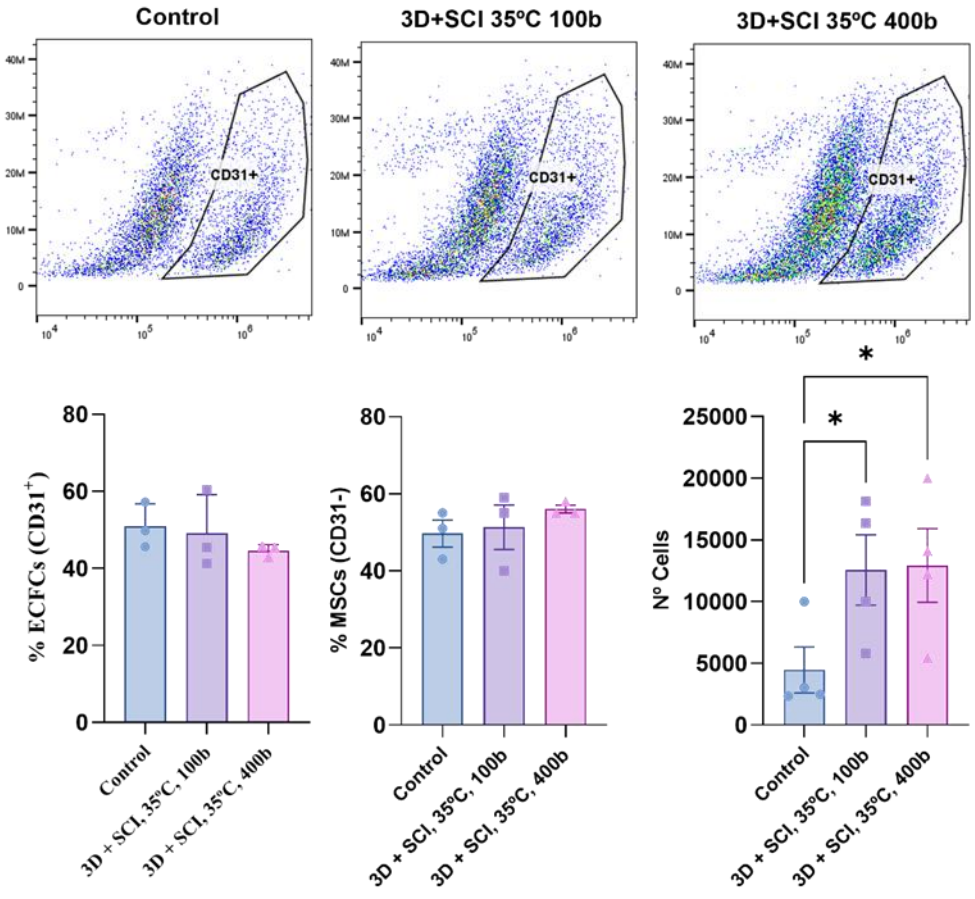

Figure 8. Effect of CD31 staining after 72 h of culture. (A) Representative dot plots for CD31 staining across conditions. (B) CD31+ cells (ECFCs). (C) CD31− cells (MSCs). (D) Total quantification of cells adherent to PLA discs. Values are presented as mean ± SEM (n = 3). P-value: * < 0.05, ** < 0.01, *** < 0.001, **** < 0.0001.

This CD31-based identification approach provides additional information beyond relative lineage proportions, specifically the total cell count per sample. As shown in Figure 8D, significant differences were detected in the total number of adherent cells on MLE impregnated PLA discs compared with unimpregnated controls, in agreement with the calcein-based viability assay. Figure 8B illustrates the percentage of CD31+ endothelial cells, which was similar across all conditions. Similarly, Figure 10C shows the percentage of CD31− mesenchymal cells, defined as the population

 doi:10.20944/preprints202603.0072.v1

lacking CD31 staining. Overall, the proportion of each cell type per well did not vary substantially relative to the control.

Taken together, these findings support the conclusion that MLE impregnated PLA discs generated a more favorable environment for the maintenance and growth of both endothelial and mesenchymal cells [32] without apparent selectivity. In other words, within the conditions tested, MLE impregnated PLA supported ECFCs and MSCs in comparable proportions, consistent with balanced co culture maintenance.

Finally, the influence of extract concentration on the apoptosis of ECFCs and MSCs was also evaluated by flow cytometry. No statistically significant differences were observed in early or late apoptosis between control and impregnated discs (Figure 9B and 9C). However, a trend toward reduced late apoptosis was observed in the impregnated discs, potentially linked to anti apoptotic properties attributed to mango leaf extract in both cell types [32]. This trend may also suggest that the extract concentration was insufficient to elicit a clear anti apoptotic effect [49], a conclusion that is conceptually consistent with the findings from the proliferation assay.

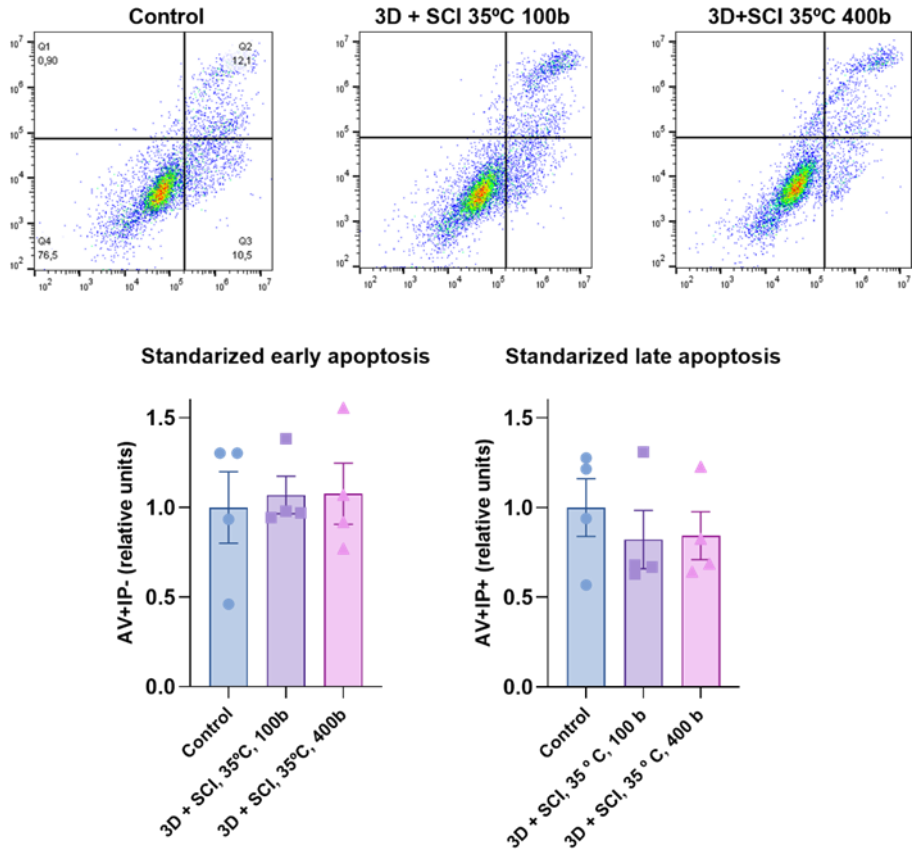

Figure 9. Effect of mango leaf extract on apoptosis of ECFCs + MSCs. (A) Representative dot plots showing apoptosis profiles of ECFCs + MSCs seeded on PLA discs under different conditions: (1) 3D + SCI, T = 35 °C, P = 100 bar; (2) 3D + SCI, T = 35 °C, P = 400 bar; (3) Control. (B, C) Graphs show the effect of MLE contained in PLA discs impregnated under different conditions on normalized early and late apoptosis. Values are presented as mean ± SEM (n = 3).

4. Conclusions

This study demonstrates that MLE can be successfully incorporated into PLA using $scCO_2$ assisted impregnation, yielding a biofunctionalized and cytocompatible material. Enhanced solvent extraction produced an MLE fraction with high antioxidant capacity, supporting its suitability as a

 doi:10.20944/preprints202603.0072.v1

natural source of bioactive compounds for polymer functionalization (Mustafa and Turner, 2011; Fernández Ponce et al., 2017; Scherer and Godoy, 2009).

A key outcome of this work is that the manufacturing sequence is the dominant determinant of both material fidelity and functional performance. The workflow based on 3D printing followed by impregnation (3D + SCI) preserved disc geometry and enabled higher MLE loading than impregnation prior to printing (SCI + 3D). Thie latter was associated with filament instability, disc deformation, and reduced effective cell colonization.

From a biological standpoint, MLE impregnated PLA produced under the 3D + SCI workflow, particularly at 35 °C and 400 bar, supported increased adhesion and viability of ECFCs and MSCs, and enhanced the proliferative fraction in co culture, while maintaining comparable lineage proportions as assessed by CD31 flow cytometry. Furthermore, apoptosis analysis did not indicate pro apoptotic effects under the tested conditions, supporting the material's cytocompatibility.

Overall, these findings position post-printing supercritical impregnation as a robust, green and reproducible strategy to generate antioxidant PLA constructs from agro- industrial by products. This approach holds significant potential for vascular-oriented tissue engineering and regenerative applications. Future studies should define the release kinetics and stability of the bioactive fraction, establish the concentration range at which MLE shifts toward anti-proliferative or anti-apoptotic effects, and expand functional endpoints and mechanical characterization to strengthen translational readiness (Cells et al., 2022; Goodman et al., 2013; Jiang et al., 2020).

Author Contributions: Conceptualization, LCC, CMS, ISG and MCDR; methodology, ISG, MCM and CCB; formal analysis, ISG, CCB and MCM; resources, LCC, CMS and MCDR; data curation, ISG, LCC and MCDR.; writing—original draft preparation, ISG and MCM; writing—review and editing, ISG, LCC, MCDR; visualization, ISG and MCM; supervision, LCC, CMS and MCDR; funding acquisition, LCC, CMS, MCDR and ISG. All authors have read and agreed to the published version of the manuscript.".

Funding.: This study was supported by the Institute of Health Carlos III, ISCIII (PI20-00716, PI24-01161), co-funded by European Regional Development Fund "A way to make Europe"; and the PAIDI-RETOS (PI20-00932), Junta de Andalucía; and by the project PR2023-018 (reference 2023-014/PU/PP-PR-IMP-NOV/PR), from Research Projects call (Investigador Novel), University of Cádiz, UCA-IN.,.

Informed Consent Statement: Not applicable.

Conflicts of Interest: The authors declare no conflicts of interest.

Abbreviations

The following abbreviations are used in this manuscript:

AAI	Antioxidant activity index
AN V	Annexin V
CO_2	Carbon dioxide
DAPI	4',6 diamidino 2 phenylindole
DPPH	2,2 diphenyl 1 picrylhydrazyl
ECFCs	Endothelial colony forming cells
EGM 2	Endothelial Growth Medium 2
FBS	Fetal bovine serum
GPS	Glutamine penicillin streptomycin
IC_{50}	Half maximal inhibitory concentration
MLE	Mango leaf extract
MSCs	Mesenchymal stromal cells
PBS	Phosphate buffered saline
PBT	PBS with Triton X 100
PI	Propidium iodide
PLA	Poly(lactic acid)
PFA	Paraformaldehyde

 doi:10.20944/preprints202603.0072.v1

SCI Supercritical impregnation

References

1. Ulery, B.D.; Nair, L.S.; Laurencin, C.T. Biomedical Applications of Biodegradable Polymers. *J. Polym. Sci. B Polym. Phys.* 2011, *49*.
2. Tabernero, A.; González-Garcinuño, Á.; Cardea, S.; Martín del Valle, E. Supercritical Carbon Dioxide and Biomedicine: Opening the Doors towards Biocompatibility. *Chemical Engineering Journal* **2022**, *444*, 136615, doi:10.1016/J.CEJ.2022.136615.
3. Liu, S.; Wu, G.; Zhang, X.; Yu, J.; Liu, M.; Zhang, Y.; Wang, P.; Yin, X.; Zhang, J.; Li, F.; et al. Preparation and Properties of Poly (Lactic Acid) (PLA) Suture Loaded with PLA Microspheres Enclosed Drugs (PM-Ds). *Journal of the Textile Institute* **2019**, *110*, 1596–1605, doi:10.1080/00405000.2019.1610999;CTYPE:STRING:JOURNAL.
4. Luo, G.; Zhang, Y.; Chen, P.; Wu, F.; Shi, M.; Ma, Y.; Wang, X. Tailoring Osteo-Immunomodulatory Micro-Environments via a Bioactive 3D PLA Scaffold to Potentiate Regenerative Healing. *Colloids Surf. B Biointerfaces* **2025**, *253*, 114711, doi:10.1016/J.COLSURFB.2025.114711.
5. Liu, Q.; Bi, C.; Hu, H.; Zhang, Z.; Zhang, B. Reduction of Amylose/Amylopectin Ratio Improves the Molecular Orientation and Performance of Three-Dimensional-Printed Thermoplastic Starch/Polylactic Acid Intestinal Stents. *Int. J. Biol. Macromol.* **2025**, *308*, 142419, doi:10.1016/J.IJBIOMAC.2025.142419.
6. Faal, M.; Faal, M.; Ahmadi, T.; Dehgan, F. Fabrication and Evaluation of Polylactic Acid-Curcumin Containing Carbon Nanotubes (CNTs) Wound Dressing Using Electrospinning Method with Experimental and Computational Approaches. *Scientific Reports 2025 15:1* **2025**, *15*, 13398-, doi:10.1038/s41598-025-98393-2.
7. Shi, Y.; Li, D.; Hill, C.; Yang, L.; Sheerin, E.D.; Pilliadugula, R.; Wang, J.J.; Boland, J.; Xiao, L. Micro and Nano Plastics Release from a Single Absorbable Suture into Simulated Body Fluid. *J. Hazard. Mater.* **2024**, *466*, 133559, doi:10.1016/J.JHAZMAT.2024.133559.
8. Seegobin, N.; Abdalla, Y.; Li, G.; Murdan, S.; Shorthouse, D.; Basit, A.W. Optimising the Production of PLGA Nanoparticles by Combining Design of Experiment and Machine Learning. *Int. J. Pharm.* **2024**, *667*, 124905, doi:10.1016/J.IJPHARM.2024.124905.
9. Tong, L.; Shi, G.; Liu, Q.; Qian, Z.; Li, J.; Zhang, K.; Zhu, Y.; Fang, Y.; Sha, L.; Bai, L.; et al. Fabrication and Evaluation of 3D Printed PLGA/NHA/GO Scaffold for Bone Tissue Engineering. *Scientific Reports 2025 15:1* **2025**, *15*, 12446-, doi:10.1038/s41598-025-96099-z.
10. Lin, Y.; Zhao, L.; Jin, H.; Gu, Q.; Lei, L.; Fang, C.; Pan, X. Multifunctional Applications of Silk Fibroin in Biomedical Engineering: A Comprehensive Review on Innovations and Impact. *Int. J. Biol. Macromol.* **2025**, *309*, 143067, doi:10.1016/J.IJBIOMAC.2025.143067.
11. Peiravi, M.; Sherafat, Z.; Sani, M.; Azarpira, N. In Vitro and in Vivo Assessment of 3D-Printed PCL/PLA/ZnO Nanocomposite Scaffolds for Osteoarthritis Treatment. *Composites Communications* **2025**, *57*, 102432, doi:10.1016/J.COCO.2025.102432.
12. Teng, Y.; Wang, X.; Song, L.; Yang, J.; Hou, S.; Lv, Q.; Jiang, L.; Guan, Y.; Shi, J. 3D Printed Polycaprolactone/Poly (L-Lactide-Co-ε-Caprolactone) Composite Ureteral Stent with Biodegradable and Antibacterial Properties. *Biomedical Materials* **2025**, *20*, 025026, doi:10.1088/1748-605X/ADB2CE.
13. Demartis, S.; Picco, C.J.; Larrañeta, E.; Korelidou, A.; Islam, R.; Coulter, J.A.; Giunchedi, P.; Donnelly, R.F.; Rassu, G.; Gavini, E. Evaluating the Efficacy of Rose Bengal-PVA Combinations within PCL/PLA Implants for Sustained Cancer Treatment. *Drug Delivery and Translational Research 2024 15:5* **2024**, *15*, 1770–1785, doi:10.1007/S13346-024-01711-W.
14. Obiweluozor, F.O.; Kayumov, M.; Kwak, Y.; Cho, H.J.; Park, C.H.; Park, J. kyu; Jeong, Y.J.; Lee, D.W.; Kim, D.W.; Jeong, I.S. Rapid Remodeling Observed at Mid-Term in-Vivo Study of a Smart Reinforced Acellular Vascular Graft Implanted on a Rat Model. *Journal of Biological Engineering 2022 17:1* **2023**, *17*, 1-, doi:10.1186/S13036-022-00313-9.
15. Stramiello, J.A.; Mohammadzadeh, A.; Ryan, J.; Brigger, M.T. The Role of Bioresorbable Intraluminal Airway Stents in Pediatric Tracheobronchial Obstruction: A Systematic Review. *Int. J. Pediatr. Otorhinolaryngol.* **2020**, *139*, 110405, doi:10.1016/J.IJPORL.2020.110405.

 doi:10.20944/preprints202603.0072.v1

16. Pandey, A.; Adama, N.; Adjallé, K.; Blais, J.F. Sustainable Applications of Polyhydroxyalkanoates in Various Fields: A Critical Review. *Int. J. Biol. Macromol.* **2022**, *221*, 1184–1201, doi:10.1016/J.IJBIOMAC.2022.09.098.
17. Ren, Z.W.; Wang, Z.Y.; Ding, Y.W.; Dao, J.W.; Li, H.R.; Ma, X.; Yang, X.Y.; Zhou, Z.Q.; Liu, J.X.; Mi, C.H.; et al. Polyhydroxyalkanoates: The Natural Biopolyester for Future Medical Innovations. *Biomater. Sci.* **2023**, *11*, 6013–6034, doi:10.1039/D3BM01043K.
18. Santhamoorthy, M.; Kim, S.C. A Review of the Development of Biopolymer Hydrogel-Based Scaffold Materials for Drug Delivery and Tissue Engineering Applications. *Gels 2025, Vol. 11,* **2025**, *11*, doi:10.3390/GELS11030178.
19. Scaffaro, R.; Botta, L.; Sanfilippo, M.; Gallo, G.; Palazzolo, G.; Puglia, A.M. Combining in the Melt Physical and Biological Properties of Poly(Caprolactone) and Chlorhexidine to Obtain Antimicrobial Surgical Monofilaments. *Applied Microbiology and Biotechnology 2012 97:1* **2012**, *97*, 99–109, doi:10.1007/S00253-012-4283-X.
20. Iqbal, J.; Gunn, J.; Serruys, P.W. Coronary Stents: Historical Development, Current Status and Future Directions. *Br. Med. Bull.* **2013**, *106*, 193–211, doi:10.1093/BMB/LDT009.
21. Soluri, A.; Hui, A.; Jones, L. Delivery of Ketotifen Fumarate by Commercial Contact Lens Materials. *Optom. Vis. Sci.* **2012**, *89*, 1140–1149, doi:10.1097/OPX.0B013E3182639DC8.
22. Davies, O.R.; Lewis, A.L.; Whitaker, M.J.; Tai, H.; Shakesheff, K.M.; Howdle, S.M. Applications of Supercritical CO_2 in the Fabrication of Polymer Systems for Drug Delivery and Tissue Engineering. *Adv. Drug Deliv. Rev.* **2008**, *60*, 373–387, doi:10.1016/J.ADDR.2006.12.001.
23. Beckman, E.J. Supercritical and Near-Critical CO_2 in Green Chemical Synthesis and Processing. *J. Supercrit. Fluids* **2004**, *28*, 121–191, doi:10.1016/S0896-8446(03)00029-9.
24. Dendoncker, K.; Putzeys, G.; Nieuwenhuizen, T.; Voet, P.; Lambrecht, S.; Bertrand, M.; Valster, H.; Croes, K. Struggling with a Cefazolin Impregnation Protocol of Bone Chips. *Cell and Tissue Banking 2025 26:2* **2025**, *26*, 11-, doi:10.1007/S10561-025-10164-5.
25. do Nascimento, U.S.; Neves, C.K.; Santos, E.F. dos; Ezegbe, C.A.; Rezende, L.R.; Marchi, J.; Lombello, C.B.; Maia-Obi, L.P. Ibuprofen Loaded Gelatin-Siloxane Gels Prepared by Supercritical CO_2-Assisted Impregnation/Deposition for Controlled Drug Release and Tissue Engineering. *J. Supercrit. Fluids* **2025**, *218*, 106511, doi:10.1016/J.SUPFLU.2024.106511.
26. Yamamoto, K.; Ushiki, I. Impregnation of Non-Steroidal Anti-Inflammatory Drugs (Ibuprofen and Ketoprofen) onto Mesoporous Silica SBA-15 Using Supercritical CO_2. *Journal of CO_2 Utilization* **2025**, *92*, 103022, doi:10.1016/J.JCOU.2025.103022.
27. Erdogan, H.; Gungor, B.; Suner, S.S.; Silan, C.; Saraydin, S.U.; Saraydin, D.; Ayyala, R.S.; Sahiner, N. Moxifloxacin-Impregnated Contact Lenses for Treatment of Keratitis in Rabbit Eyes. *Polym. Adv. Technol.* **2025**, *36*, e70134, doi:10.1002/PAT.70134.
28. Machado, N.D.; Cejudo-Bastante, C.; Goñi, M.L.; Gañán, N.A.; Casas-Cardoso, L.; Mantell-Serrano, C. Screening of the Supercritical Impregnation of Olea Europaea Leaves Extract into Filaments of Thermoplastic Polyurethane (TPU) and Polylactic Acid (PLA) Intended for Biomedical Applications. *Antioxidants 2022, Vol. 11,* **2022**, *11*, doi:10.3390/ANTIOX11061170.
29. Verano-Naranjo, L.; Cejudo-Bastante, C.; Casas, L.; Martínez de la Ossa, E.; Mantell, C. Use of Winemaking By-Products for the Functionalization of Polylactic Acid for Biomedical Applications. *Antioxidants 2023, Vol. 12,* **2023**, *12*, doi:10.3390/ANTIOX12071416.
30. Khumpook, T.; Saenphet, S.; Tragoolpua, Y.; Saenphet, K. Anti-Inflammatory and Antioxidant Activity of Thai Mango (Mangifera Indica Linn.) Leaf Extracts. *Comparative Clinical Pathology 2018 28:1* **2018**, *28*, 157–164, doi:10.1007/S00580-018-2809-Z.
31. Jiang, T.; Han, F.; Gao, G.; Liu, M. Mangiferin Exert Cardioprotective and Anti-Apoptotic Effects in Heart Failure Induced Rats. *Life Sci.* **2020**, *249*, 117476, doi:10.1016/J.LFS.2020.117476.
32. Sánchez-Gomar, I.; Benítez-Camacho, J.; Cejudo-Bastante, C.; Casas, L.; Moreno-Luna, R.; Mantell, C.; Durán-Ruiz, M.C. Pro-Angiogenic Effects of Natural Antioxidants Extracted from Mango Leaf, Olive Leaf and Red Grape Pomace over Endothelial Colony-Forming Cells. *Antioxidants 2022, Vol. 11,* **2022**, *11*, doi:10.3390/ANTIOX11050851.

33. Rosales, J.M.; Cejudo, C.; Verano, L.; Casas, L.; Mantell, C.; Martínez de la Ossa, E.J. Supercritical Impregnation of PLA Filaments with Mango Leaf Extract to Manufacture Functionalized Biomedical Devices by 3D Printing. *Polymers 2021, Vol. 13*, **2021**, *13*, doi:10.3390/POLYM13132125.
34. Fernández-Ponce, M.T.; Casas, L.; Mantell, C.; Martínez De La Ossa, E.J. Use of high pressure techniques to produce Mangifera indica L. leaf extracts enriched in potent antioxidant phenolic compounds. Innov. *Food Sci. Emerg. Technol Food Funct.* **2015**, *29*, 94-106, doi:10. 1016/j.ifset.2015.04.006.
35. Brand-Williams, W.; Cuvelier, M.E.; Berset, C. Use of a Free Radical Method to Evaluate Antioxidant Activity. *LWT - Food Science and Technology* **1995**, *28*, 25–30, doi:10.1016/S0023-6438(95)80008-5.
36. Scherer, R.; Godoy, H.T. Antioxidant Activity Index (AAI) by the 2,2-Diphenyl-1-Picrylhydrazyl Method. *Food Chem.* **2009**, *112*, 654–658, doi:10.1016/J.FOODCHEM.2008.06.026.
37. Lin, R.Z.; Chen, Y.C.; Moreno-Luna, R.; Khademhosseini, A.; Melero-Martin, J.M. Transdermal Regulation of Vascular Network Bioengineering Using Aphotopolymerizable Methacrylated Gelatin Hydrogel. *Biomaterials* **2013**, *34*, 6785–6796, doi:10.1016/j.biomaterials.2013.05.060.
38. Grosso, P.; Cejudo, C.; Sánchez-Gomar, I.; Durán-Ruiz, M.ª. C.; Moreno-Luna, R.; Casas, L.; Pereyra, C.; Mantell, C. Supercritical Impregnation of Mango Leaf Extract into PLA 3D-Printed Devices and Evaluation of Their Biocompatibility with Endothelial Cell Cultures. *Polymers 2022, Vol. 14*, **2022**, *14*, doi:10.3390/POLYM14132706.
39. Mustafa, A.; Turner, C. Pressurized Liquid Extraction as a Green Approach in Food and Herbal Plants Extraction: A Review. *Anal. Chim. Acta* **2011**, *703*, 8–18, doi:10.1016/J.ACA.2011.07.018.
40. Fernández-Ponce, M.T.; López-Biedma, A.; Sánchez-Quesada, C.; Casas, L.; Mantell, C.; Gaforio, J.J.; Martínez De La Ossa, E.J. Selective Antitumoural Action of Pressurized Mango Leaf Extracts against Minimally and Highly Invasive Breast Cancer. *Food Funct.* **2017**, *8*, 3610–3620, doi:10.1039/C7FO00877E.
41. Zhang, J.; Wu, H. Valorization of Bioactive Compounds from Food By-Products Using Supercritical Fluid Extraction: A Technological and Industrial Perspective. *Food Chem.* **2025**, *484*, 144277, doi:10.1016/J.FOODCHEM.2025.144277.
42. de Araujo, E.J.S.; Martínez, J. Scenarios, Prospects, and Challenges Related to Supercritical Fluid Impregnation in the Food Industry: A Scoping Review (2018–2023). *Biofuels, Bioproducts and Biorefining* **2024**, *18*, 2091–2115, doi:10.1002/BBB.2671;WGROUP:STRING:PUBLICATION.
43. Reed, K.E.; Westphale, E.M.; Larson, D.M.; Wang, H.Z.; Veenstra, R.D.; Beyer, E.C. Molecular Cloning and Functional Expression of Human Connexin37, an Endothelial Cell Gap Junction Protein. *J. Clin. Invest.* **1993**, *91*, 997–1004, doi:10.1172/JCI116321.
44. Brighton, C.T.; Hunt, R.M. Early Histological and Ultrastructural Changes in Medullary Fracture Callus. *Journal of Bone and Joint Surgery - Series A* **1991**, *73*, doi:10.2106/00004623-199173060-00006.
45. Ismail, M.B.; Rajendran, P.; Zahra, H.M.A.; Veeraraghavan, V.P. Mangiferin Inhibits Apoptosis in Doxorubicin-Induced Vascular Endothelial Cells via the Nrf2 Signaling Pathway. *International Journal of Molecular Sciences 2021, Vol. 22*, **2021**, *22*, doi:10.3390/IJMS22084259.
46. Tu, J.B.; Ma, R.Z.; Dong, Q.; Jiang, F.; Hu, X.Y.; Li, Q.Y.; Pattar, P.; Zhang, H. Induction of Apoptosis in Infantile Hemangioma Endothelial Cells by Propranolol. *Exp. Ther. Med.* **2013**, *6*, 574–578, doi:10.3892/ETM.2013.1159/ABSTRACT.
47. Azizah, A.H.; Nik Ruslawati, N.M.; Swee Tee, T. Extraction and Characterization of Antioxidant from Cocoa By-Products. *Food Chem.* **1999**, *64*, 199–202, doi:10.1016/S0308-8146(98)00121-6.
48. Goodman, S.B.; Yao, Z.; Keeney, M.; Yang, F. The Future of Biologic Coatings for Orthopaedic Implants. *Biomaterials* **2013**, *34*, 3174–3183, doi:10.1016/J.BIOMATERIALS.2013.01.074.
49. Jiang, T.; Han, F.; Gao, G.; Liu, M. Mangiferin Exert Cardioprotective and Anti-Apoptotic Effects in Heart Failure Induced Rats. *Life Sci.* **2020**, *249*, 117476, doi:10.1016/J.LFS.2020.117476.